Electrocatalysis

International Edition: DOI: 10.1002/anie.201710859
German Edition: DOI: 10.1002/ange.201710859

In-Plane Black Phosphorus/Dicobalt Phosphide Heterostructure for Efficient Electrocatalysis

*Jiahong Wang, Danni Liu, Hao Huang, Na Yang, Bo Yu, Min Wen, Xin Wang, Paul K. Chu, and Xue-Feng Yu**

Abstract: *Heterostructures composed of two-dimensional black phosphorus (2D BP) with unique physical/chemical properties are of great interest. Herein, we report a simple solvothermal method to synthesize in-plane BP/Co_2P heterostructures for electrocatalysis. By using the reactive edge defects of the BP nanosheets as the initial sites, Co_2P nanocrystals are selectively grown on the BP edges to form the in-plane BP/Co_2P heterostructures. Owing to disposition on the original defects of BP, Co_2P improves the conductivity and offers more active electrocatalytic sites, so that the BP/Co_2P nanosheets exhibit better and more stable electrocatalytic activities in the hydrogen evolution and oxygen evolution reactions. Our work not only extends the application of BP to electrochemistry, but also provides a new idea to improve the performance of BP by utilization of defects. Furthermore, this strategy can be extended to produce other BP heterostructures to expand the corresponding applications.*

Black phosphorus (BP), a direct band-gap-layered semiconductor, is a burgeoning member of two-dimensional (2D) materials.[1] The intriguing physical properties such as the high charge-carrier mobility, large on/off ratio, significant anisotropy, and layer-dependent band gap have spurred tremendous interests in BP.[1b,2] BP flakes obtained by mechanical exfoliation have been studied in field-effect transistors and photoelectric devices.[2] On the heels of advance in liquid exfoliation techniques, monodispersed BP nanosheets have been synthesized, for example, for lithium-ion batteries, phototherapy, photovoltaics, sensing, and catalysis.[3] Owing to the large surface area, long charge-carrier diffusion paths, relatively high carrier mobility, and lone-pairs, BP nanosheets are potential electrocatalysts for water electrolysis to produce hydrogen and oxygen.[4] However, BP suffers from instability.[5] For example, preparation of monodispersed BP nanosheets depends on long-time ultrasonic treatment or shear exfoliation,[6] during which the BP layers are gradually cleaved and defects are generated on the edges and surface. These defects not only lead to the rapid degradation of the BP nanosheets, but also undermine the conductivity and electrochemical activity thus causing problems in many applications, especially long-term catalysis. Although some strategies have been proposed to enhance the stability of BP against degradation, it is still a challenge to cope with the defects.[7]

The design and fabrication of the desirable heterostructures is a good strategy to tailor the properties of 2D materials.[8] Because the in-plane charge carrier mobility of 2D materials is much higher than that between interlayers, in-plane heterostructures have intrinsic advantages.[9] Some interesting BP heterostructures have been fabricated by techniques such as ion implantation,[10] electron doping,[11] surface coating,[12] in situ reduction[13] and van der Waals chemistry.[14] In these heterostructures, BP is generally used to promote charge separation at the semiconductor heterojunction or improve the conductivity.[15] Very recently, a BP based 0D-2D heterostructure containing Ni_2P nanoparticles homogeneously embedded in the BP nanosheets has been prepared for Li storage and acidic hydrogen evolution.[16] However, to the best of our knowledge, the synthesis of monodispersed in-plane BP heterostructures has not been reported.

Herein, a simple solvothermal strategy is designed to synthesize in-plane black phosphorus/dicobalt phosphide (BP/Co_2P) heterostructures by defect/edge-selective growth of Co_2P on the BP nanosheets. The synthesis involves an anhydrous and oxygen-free sealed high-temperature reaction, in which the high chemical activity of the defect sites in BP enables edge-selective reduction of Co ions. Co_2P on the edges not only occupy the defects, but also provide effective electrocatalytic sites to improve the electrocatalytic activities in the hydrogen evolution reaction (HER) and oxygen evolution reaction (OER).

Figure 1 a illustrates the procedures to synthesize the BP/Co_2P heterostructures. The BP crystals are prepared by a modified chemical vapor transport method.[17] The bulk crystals are exfoliated into nanosheets in *N*-methyl-2-pyrrolidone (NMP) under sonication in a water bath. After centrifugation, the BP nanosheets are mixed with the Co ions *N*,*N*-dimethylformamide (DMF) solution in a screw-capped Teflon bottle and react at 180 °C for 4 h under Ar protection without water or oxygen. The BP/Co_2P nanosheets are obtained using careful centrifugation. As shown in the scanning electron microscopy (SEM) image in Figure 1 b, the raw bulk BP has an angular shape with a layered structure and smooth surface. The sharp (020), (040), (060), and (080) X-ray diffraction (XRD) peaks in Figure S1 (see the Supporting

[*] Dr. J. Wang, D. Liu, H. Huang, N. Yang, B. Yu, Dr. M. Wen, Dr. X. Wang, Prof. X.-F. Yu
Center for Biomedical materials and Interfaces
Shenzhen Institutes of Advanced Technology
Chinese Academy of Sciences
Shenzhen 518055 (P. R. China)
E-mail: xf.yu@siat.ac.cn
Prof. P. K. Chu
Department of Physics and Department of Materials Science and Engineering, City University of Hong Kong
Tat Chee Avenue, Kowloon, Hong Kong (China)

Supporting information and the ORCID identification number(s) for the author(s) of this article can be found under: https://doi.org/10.1002/anie.201710859.

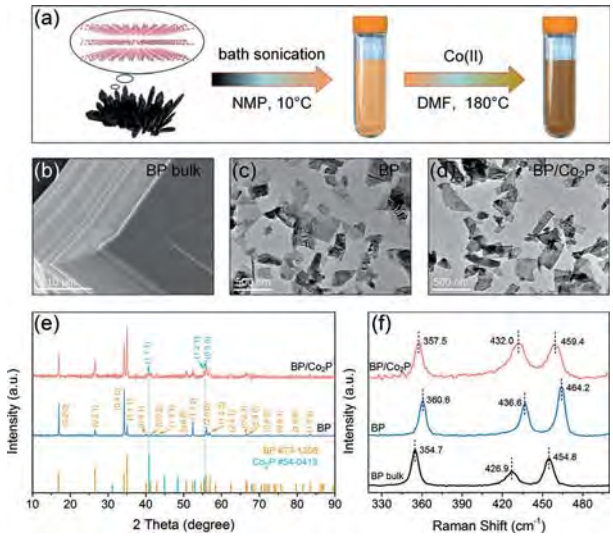

Figure 1. a) Schematic diagram of the synthesis of the BP/Co_2P heterostructures. b) SEM image of the bulk BP. c,d) TEM images of the BP and BP/Co_2P nanosheets, respectively. e) XRD patterns of the BP and BP/Co_2P nanosheets. f) Raman scattering spectra of the bulk BP as well as BP and BP/Co_2P nanosheets.

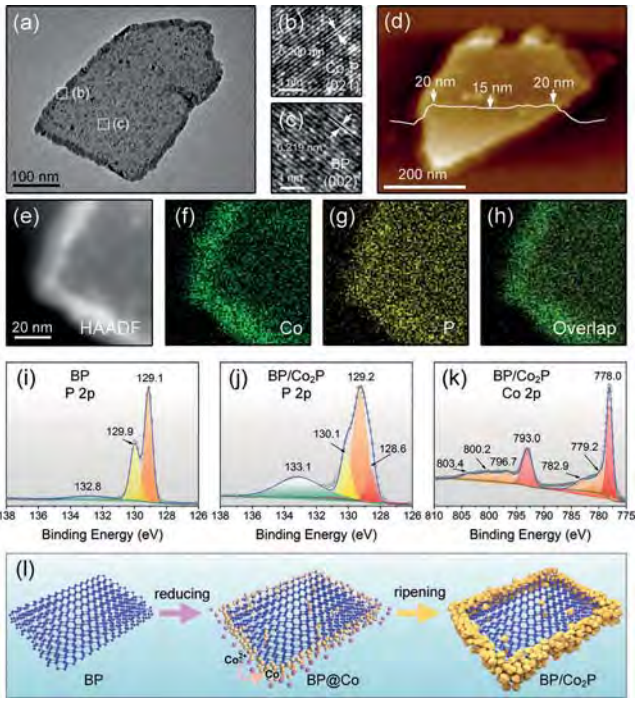

Figure 2. a) TEM image of one BP/Co_2P nanosheet. b) HR-TEM image of Co_2P corresponding to the edge location in (a). c) HR-TEM image of BP corresponding to the center position in (a). d) AFM image and line-scan of one BP/Co_2P nanosheet. e–h) HAADF image and EDS maps of one BP/Co_2P nanosheet. P 2p XPS spectra of i) BP nanosheets and j) BP/Co_2P nanosheets. k) Co 2p XPS spectrum of the BP/Co_2P nanosheets. l) Schematic diagram of the synthesis mechanism of the BP/Co_2P heterostructures.

Information) reveal the fine crystal quality. The morphology of obtained BP nanosheets with a radial dimension of about 400 nm is presented in the transmission electron microscopy (TEM) image (Figure 1c), SEM image, and atomic force microscopy (AFM) image (Figure S2). The TEM image (Figure 1d) and SEM image (Figure S3a) of BP/Co_2P disclose the planar BP and edge-modified Co_2P. Comparing the XRD patterns acquired from the BP and BP/Co_2P nanosheets, the two extra peaks at 40.8° and 55.5° (Figure 1e, Figure S4) can be indexed to the (111), (121), and (030) planes of Co_2P, where the (121) and (030) diffraction peaks completely overlap. Figure 1f shows the changes in the Raman spectra from original bulk crystals to final heterostructures. After the first-step ultrasonic exfoliation, the A_g^1 vibration mode of BP shifts from 354.7 to 360.6 cm^{-1} and both the B_{2g} and the A_g^2 peaks red-shift by about 10 cm^{-1}. The red-shift shown by the Raman peaks suggest thickness reduction and fabrication of few-layer BP nanosheets as consistent with topography revealed by AFM (Figure S2b). After Co_2P is grown on the BP nanosheets, the three characteristic peaks blue-shift due to vibrations inhibition. In particular, the in-plane vibrations of B_{2g} and A_g^2 modes blue-shift larger than the out-of-plane vibration of A_g^1 mode, demonstrating that Co_2P is mainly produced on the edges of the BP nanosheets.

The morphology of the heterostructures is shown in the magnified TEM image (Figure 2a) and edge modification produces a 15 nm wide border. The component distribution is determined by high-resolution TEM (HR-TEM; Figures 2b and c). The 0.200 nm lattice spacing of the border corresponds to the (021) crystal facet of Co_2P and the typical (002) facet of BP is found from the central area of the nanosheet. Unlike the flat BP nanosheets, BP/Co_2P displays uplifted edges in the AFM graph (Figure 2d). The uplifted edges demonstrate lattice rearrangement during the formation of Co_2P. In the localized high angle circular dark field (HAADF) image (Figure 2e), recognizable contrast can be observed similar to the TEM and AFM images. The energy-dispersive X-ray spectroscopy (EDS) maps disclose the elemental distributions in the heterostructures. Co mainly occupies the edges of the hetero-nanosheets, whereas P is evenly distributed across the entire area (Figure 2f–h). The P/Co atomic ratio of BP/Co_2P is close to 5:1 as shown in the EDS spectrum (Figure S3b) and that at the edge is about 2:1 (Figures S3c and S3d). The results confirm edge-selective growth of Co_2P and show that the ratio of BP to Co_2P is about 9:1 in the heterostructures. TEM and EDS confirm that Co_2P is mostly generated on the edges of the BP nanosheets and only a small amount is formed on the central surface. X-ray photoelectron spectroscopy (XPS) is employed to determine the chemical states of the BP/Co_2P heterostructures and Figures 2i and j display the P 2p spectra before and after Co_2P modification, respectively. The two unchanged peaks near 129 and 130 eV verify the original state of BP and the weak oxidation peak at 133 eV may arise from the solvent in the reaction. The most important change related to P is the new peak at 128.6 eV which indicates a negative valence of P. The Co 2p XPS spectra (Figure 2k) of BP/Co_2P show the Co $2p_{3/2}$ and $2p_{1/2}$ peaks at 778.0 eV and 793.0 eV, respectively, which are located between the metallic and oxidized binding energies of Co. These results are similar to those reported previously thereby corroborating the formation of Co_2P.[18]

The proposed reaction mechanism of the edge-selective synthesis of the in-plane heterostructure of BP/Co_2P is presented (Figure 2l). During liquid exfoliation, defects are inevitably produced on the BP nanosheets. The defects result in unsaturated P having a smaller coordination number, more lone electrons, and higher reducing activity. Furthermore, according to first-principles calculation reported previously, the defect occupation energy of Co (−7.65 eV) is lower than the surface adsorption energy (−4.41 eV).[19] Therefore, Co ions can be easily reduced to Co atoms on the defect sites. In addition, as the Co atoms are generated, they probably bond with adjacent P atoms. Because the coordination number (three) and bond length (about 2.3 Å) are more similar to those of Co_2P compared to CoP,[18–20] lattice rearrangement, crystallization and continuous ripening of Co_2P takes place. Since the unsaturated P and defects are usually enriched on the BP edges,[21] formation of Co_2P tends to take place at the edges as well. Furthermore, the results of the control experiments in Figure S5 and S6 show the contribution of the defect occupied by Co on the morphology retention of the BP nanosheets, and demonstrate the importance of the anhydrous and oxygen-free sealed reaction conditions.

BP nanosheets have a large potential in electrocatalysis due to the large surface area, high carrier mobility, and active lone pairs.[4] The Co_2P on the edges not only occupies the BP defects to enhance the stability, but also improves the electrocatalytic properties of the BP/Co_2P heterostructures. The HER performance of BP/Co_2P is evaluated in 0.5 M H_2SO_4 and 1.0 M KOH electrolytes. As shown by the linear sweep voltammetry (LSV) curves in Figure 3a, BP/Co_2P is highly efficient HER electrocatalyst in 0.5 M H_2SO_4 as indicated by the onset overpotential of 105 mV which is much lower than that of BP of 389 mV. Moreover, BP/Co_2P shows 100 mA cm^{-2} at an overpotential of 340 mV while BP needs a 600 mV overpotential to drive 0.3 mA cm^{-2} in 0.5 M H_2SO_4. BP/Co_2P also exhibits more superior HER behavior than BP in 1.0 M KOH with an onset overpotential of 173 mV and requiring 336 mV overpotential to achieve 100 mA cm^{-2}. Figure 3b shows that the Tafel slopes of BP/Co_2P are 62 and 72 mV/dec in 0.5 M H_2SO_4 and 1.0 M KOH, respectively, which are less than those of BP (125 and 188 mV/dec). The multi-potential curve of BP/Co_2P in 0.5 M H_2SO_4 is shown in Figure S7. When the potential increases from 210 to 250 mV, the current density levels off at 6.5 mA cm^{-2} and remains unchanged for the remaining 200 s. The trends of all the current densities are similar indicating excellent conductivity and transport properties of the BP/Co_2P electrode. The electrochemical impedance spectroscopy (EIS) results in Figure 3c compare the conductivity between the BP and BP/Co_2P electrodes. The semicircular diameter of BP/Co_2P is smaller than that of BP indicating a smaller charge transfer resistance and faster reaction rate of BP/Co_2P. Furthermore, the HER stability test results in Figure 3d indicate that BP/Co_2P has superior durability. The current density remains constant in 0.5 M H_2SO_4 and remains at 81% in 1.0 M KOH after electrolysis for 24 hours. The results confirm the excellent stability of BP/Co_2P as electrocatalysts.

The OER activities of BP/Co_2P, BP, and RuO_2 with the same loading mass are evaluated in 1.0 M KOH at a scanning rate of 5 mV s^{-1}. As shown in Figure 4a, the OER current of

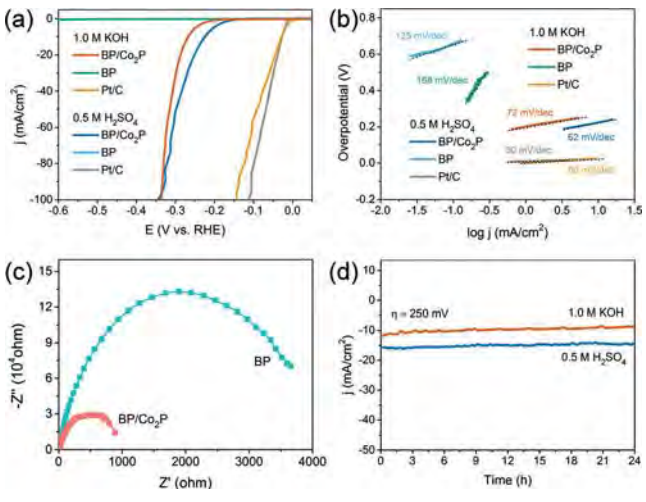

Figure 3. a) HER polarization curves of BP, BP/Co_2P, and Pt/C in 0.5 M H_2SO_4 and 1.0 M KOH. b) Corresponding Tafel plots of BP, BP/Co_2P, and Pt/C of the HER polarization curves. c) EIS curves of the BP and BP/Co_2P nanosheets. d) Stability assessment of BP/Co_2P in 0.5 M H_2SO_4 and 1.0 M KOH at 250 mV.

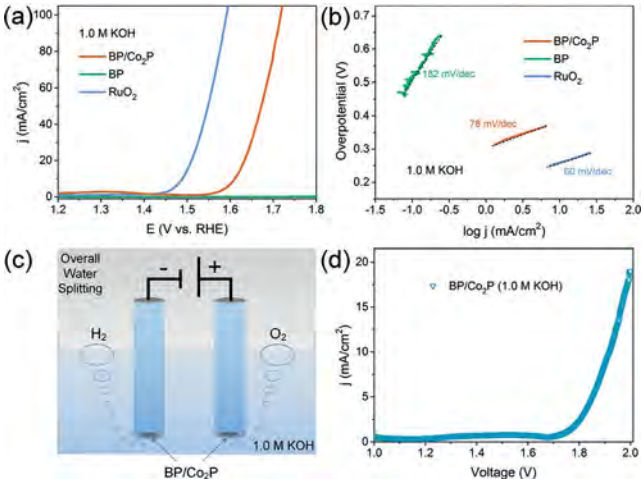

Figure 4. a) OER polarization curves of BP, BP/Co_2P, and RuO_2 in 1.0 M KOH. b) Corresponding Tafel plots of BP, BP/Co_2P, and RuO_2 of the OER polarization curves. c) Overall water splitting schematic diagram of BP/Co_2P. d) Polarization curve of BP/Co_2P for water splitting in 1.0 M KOH.

RuO_2 appears at a small onset overpotential whereas BP exhibits sluggish activity. In comparison, the BP/Co_2P electrode shows an enhanced anodic current in 1.0 M KOH at a low potential only requiring a potential of 517 mV to drive 100 mA cm^{-2}. The lower overpotential of BP/Co_2P at 300 mV and smaller Tafel slope of 78 mV/dec indicate the efficient OER activity of BP/Co_2P. Considering the superior performance of BP/Co_2P in HER and OER, a two-electrode system is fabricated with BP/Co_2P serving as both the cathode and anode to measure the overall water splitting activity in 1.0 M KOH (BP/Co_2P || BP/Co_2P) (Figure 4c). The BP/Co_2P || BP/

Co_2P needs 1.92 V to obtain 10 mA cm^{-2} in the polarization curve demonstrating that BP/Co_2P has immense potential as a water splitting catalyst (Figure 4d).

The results described here show improved electro-catalytic performance of BP/Co_2P compared to BP, the electrocatalytic activity of BP/Co_2P is also better than that observed from the Co_2P electrocatalyst with the same loading mass (Tables S1–S3).[22] The corresponding mechanisms are proposed. On account of the higher in-plane conductivity than interlayer conductivity, the electrocatalytic activity of 2D materials is mainly along the in-plane direction and so the electrocatalytic sites on the edges are most efficient.[4a,23] Here, Co_2P prepared on the BP edges serves as active site and thus increases the number of active sites on the edges. The charge carrier concentration and electrical conductivity of the nanosheets are improved by Co_2P and the possible Co induced N-doping. The lifted edges of the heterostructures prevent stacking of the nanosheets to facilitate active sites exposure and gas effusion. Last but not least, the Co imbedded on the interface between BP and Co_2P may provide more active sites due to the synergetic effects of BP and Co_2P.

In conclusion, in-plane BP/Co_2P heterostructures have been synthesized by in situ reduction of Co on the BP defect/edge sites. Owing to occupation of the original defects, the anchored Co_2P improves the electrical conductivity and active electrocatalytic sites enabling the BP/Co_2P nanosheets to deliver stable and excellent HER and OER performances even under a large potential and current density. Considering that defects affect the properties and stability of BP, proper utilization of defects is a new and efficient strategy to improve the stability and performance of BP nanosheets. As a wet chemical method to prepare monodispersed and in-plane BP heterostructures, it can be extended to produce other BP-based nanocomposites to expand to corresponding applications.

Acknowledgements

This work was jointly supported by the National Natural Science Foundation of China (grant numbers 51702352 and 51672305), China Postdoctoral Science Foundation (grant number 2017M612762), Key Research Program of Frontier Sciences, CAS (grant number QYZDB-SSW-SLH034), Science and Technology Key Project of Shenzhen (grant number JCYJ20140417113430608), Leading Talents of Guangdong Province Program (grant number 00201520), Hong Kong Research Grants Council (RGC) General Research Funds (GRF grant number CityU 11301215), and City University of Hong Kong Strategic Research Grant (SRG grant number 7004644).

Conflict of interest

The authors declare no conflict of interest.

Keywords: black phosphorus · electrocatalysis · heterostructures · phosphorene · two-dimensional materials

How to cite: *Angew. Chem. Int. Ed.* **2018**, *57*, 2600–2604
Angew. Chem. **2018**, *130*, 2630–2634

[1] a) L. Li, Y. Yu, G. J. Ye, Q. Ge, X. Ou, H. Wu, D. Feng, X. H. Chen, Y. Zhang, *Nat. Nanotechnol.* **2014**, *9*, 372–377; b) X. Ling, H. Wang, S. Huang, F. Xia, M. S. Dresselhaus, *Proc. Natl. Acad. Sci. USA* **2015**, *112*, 4523–4530.
[2] H. Liu, Y. Du, Y. Deng, P. D. Ye, *Chem. Soc. Rev.* **2015**, *44*, 2732–2743.
[3] Y. Yi, X.-F. Yu, W. Zhou, J. Wang, P. K. Chu, *Mater. Sci. Eng. R* **2017**, *120*, 1–33.
[4] a) Z. Sofer, D. Sedmidubský, Š. Huber, J. Luxa, D. Bouša, C. Boothroyd, M. Pumera, *Angew. Chem. Int. Ed.* **2016**, *55*, 3382–3386; *Angew. Chem.* **2016**, *128*, 3443–3447; b) Q. Jiang, L. Xu, N. Chen, H. Zhang, L. Dai, S. Wang, *Angew. Chem. Int. Ed.* **2016**, *55*, 13849–13853; *Angew. Chem.* **2016**, *128*, 14053–14057; c) X. Ren, J. Zhou, X. Qi, Y. Liu, Z. Huang, Z. Li, Y. Ge, S. C. Dhanabalan, J. S. Ponraj, S. Wang, J. Zhong, H. Zhang, *Adv. Energy Mater.* **2017**, *7*, 1700396.
[5] O. I. Joshua, A. S. Gary, S. J. van der Zant Herre, C.-G. Andres, *2D Mater.* **2015**, *2*, 011002.
[6] a) X. Zhang, H. Xie, Z. Liu, C. Tan, Z. Luo, H. Li, J. Lin, L. Sun, W. Chen, Z. Xu, L. Xie, W. Huang, H. Zhang, *Angew. Chem. Int. Ed.* **2015**, *54*, 3653–3657; *Angew. Chem.* **2015**, *127*, 3724–3728; b) J. Kang, J. D. Wood, S. A. Wells, J. H. Lee, X. Liu, K. S. Chen, M. C. Hersam, *ACS Nano* **2015**, *9*, 3596–3604; c) Z. Guo, H. Zhang, S. Lu, Z. Wang, S. Tang, J. Shao, Z. Sun, H. Xie, H. Wang, X.-F. Yu, P. K. Chu, *Adv. Funct. Mater.* **2015**, *25*, 6996–7002.
[7] W. Lei, G. Liu, J. Zhang, M. Liu, *Chem. Soc. Rev.* **2017**, *46*, 3492–3509.
[8] a) C. Tan, Z. Zeng, X. Huang, X. Rui, X.-J. Wu, B. Li, Z. Luo, J. Chen, B. Chen, Q. Yan, H. Zhang, *Angew. Chem. Int. Ed.* **2015**, *54*, 1841–1845; *Angew. Chem.* **2015**, *127*, 1861–1865; b) F. Wang, P. He, Y. Li, T. A. Shifa, Y. Deng, K. Liu, Q. Wang, F. Wang, Y. Wen, Z. Wang, X. Zhan, L. Sun, J. He, *Adv. Funct. Mater.* **2017**, *27*, 1605802; c) B. Liu, A. Abbas, C. Zhou, *Adv. Electron. Mater.* **2017**, *3*, 1700045.
[9] C. Tan, X. Cao, X.-J. Wu, Q. He, J. Yang, X. Zhang, J. Chen, W. Zhao, S. Han, G.-H. Nam, M. Sindoro, H. Zhang, *Chem. Rev.* **2017**, *117*, 6225–6331.
[10] S. P. Koenig, R. A. Doganov, L. Seixas, A. Carvalho, J. Y. Tan, K. Watanabe, T. Taniguchi, N. Yakovlev, A. H. Castro Neto, B. Özyilmaz, *Nano Lett.* **2016**, *16*, 2145–2151.
[11] G. Wang, L. Bao, T. Pei, R. Ma, Y.-Y. Zhang, L. Sun, G. Zhang, H. Yang, J. Li, C. Gu, S. Du, S. T. Pantelides, R. D. Schrimpf, H.-j. Gao, *Nano Lett.* **2016**, *16*, 6870–6878.
[12] H. U. Lee, S. C. Lee, J. Won, B.-C. Son, S. Choi, Y. Kim, S. Y. Park, H.-S. Kim, Y.-C. Lee, J. Lee, *Sci. Rep.* **2015**, *5*, 8691.
[13] H. Huang, Q. Xiao, J. Wang, X.-F. Yu, H. Wang, H. Zhang, P. K. Chu, *npj 2D Mater. Appl.* **2017**, *1*, 20.
[14] a) R. He, J. Hua, A. Zhang, C. Wang, J. Peng, W. Chen, J. Zeng, *Nano Lett.* **2017**, *17*, 4311–4316; b) J. Sun, H.-W. Lee, M. Pasta, H. Yuan, G. Zheng, Y. Sun, Y. Li, Y. Cui, *Nat. Nanotechnol.* **2015**, *10*, 980–985.
[15] Y. Lin, Y. Pan, J. Zhang, *Int. J. Hydrogen Energy* **2017**, *42*, 7951–7956.
[16] Z.-Z. Luo, Y. Zhang, C. Zhang, H. T. Tan, Z. Li, A. Abutaha, X.-L. Wu, Q. Xiong, K. A. Khor, K. Hippalgaonkar, J. Xu, H. H. Hng, Q. Yan, *Adv. Energy Mater.* **2017**, *7*, 1601285.
[17] M. Köpf, N. Eckstein, D. Pfister, C. Grotz, I. Kruger, M. Greiwe, T. Hansen, H. Kohlmann, T. Nilges, *J. Cryst. Growth* **2014**, *405*, 6–10.
[18] J. F. Callejas, C. G. Read, E. J. Popczun, J. M. McEnaney, R. E. Schaak, *Chem. Mater.* **2015**, *27*, 3769–3774.

[19] a) S. Nawat, H. Fayyaz, Z. Gang, C. Cheng Hsin, C. Yongqing, Z. Yong-Wei, *Nanotechnology* **2016**, *27*, 065708; b) X. Sui, C. Si, B. Shao, X. Zou, J. Wu, B.-L. Gu, W. Duan, *J. Phys. Chem. C* **2015**, *119*, 10059 – 10063.

[20] D.-H. Ha, L. M. Moreau, C. R. Bealing, H. Zhang, R. G. Hennig, R. D. Robinson, *J. Mater. Chem.* **2011**, *21*, 11498 – 11510.

[21] X. Liu, J. D. Wood, K.-S. Chen, E. Cho, M. C. Hersam, *J. Phys. Chem. Lett.* **2015**, *6*, 773 – 778.

[22] a) Z. Dai, H. Geng, J. Wang, Y. Luo, B. Li, Y. Zong, J. Yang, Y. Guo, Y. Zheng, X. Wang, Q. Yan, *ACS Nano* **2017**, *11*, 11031 – 11040; b) D. Das, K. K. Nanda, *Nano Energy* **2016**, *30*, 303 – 311; c) Y. Hou, Y. Liu, R. Gao, Q. Li, H. Guo, A. Goswami, R. Zboril, M. B. Gawande, X. Zou, *ACS Catal.* **2017**, *7*, 7038 – 7042; d) Z. Huang, Z. Chen, Z. Chen, C. Lv, M. G. Humphrey, C. Zhang, *Nano Energy* **2014**, *9*, 373 – 382; e) J. Wang, W. Yang, J. Liu, *J. Mater. Chem. A* **2016**, *4*, 4686 – 4690; f) K. Xu, H. Ding, M. Zhang, M. Chen, Z. Hao, L. Zhang, C. Wu, Y. Xie, *Adv. Mater.* **2017**, *29*, 1606980; g) Y. Yang, X. Liang, F. Li, S. Li, X. Li, S. P. Ng, C. L. Wu, R. Li, *ChemSusChem* **2017**, DOI: 10.1002/cssc.201701705; h) M. Zhuang, X. Ou, Y. Dou, L. Zhang, Q. Zhang, R. Wu, Y. Ding, M. Shao, Z. Luo, *Nano Lett.* **2016**, *16*, 4691 – 4698.

[23] a) T. F. Jaramillo, K. P. Jorgensen, J. Bonde, J. H. Nielsen, S. Horch, I. Chorkendorff, *Science* **2007**, *317*, 100 – 102; b) H. Li, C. Tsai, A. L. Koh, L. Cai, A. W. Contryman, A. H. Fragapane, J. Zhao, H. S. Han, H. C. Manoharan, F. Abild-Pedersen, J. K. Norskov, X. Zheng, *Nat. Mater.* **2016**, *15*, 364; c) M. A. Lukowski, A. S. Daniel, F. Meng, A. Forticaux, L. Li, S. Jin, *J. Am. Chem. Soc.* **2013**, *135*, 10274 – 10277; d) Y. Zhang, K. Liu, F. Wang, T. A. Shifa, Y. Wen, F. Wang, K. Xu, Z. Wang, C. Jiang, J. He, *Nanoscale* **2017**, *9*, 5641 – 5647.

Manuscript received: October 22, 2017
Revised manuscript received: December 8, 2017
Accepted manuscript online: December 19, 2017
Version of record online: February 5, 2018

